Journal of Applied Physics

10 to 25-fold increase in the transport superconducting critical current density of spark-plasma sintered Bi-2223 superconductors

Cite as: J. Appl. Phys. **117**, 043903 (2015); https://doi.org/10.1063/1.4906560
Submitted: 25 November 2014 . Accepted: 14 January 2015 . Published Online: 26 January 2015

E. Govea-Alcaide, I. F. Machado, and R. F. Jardim

10 to 25-fold increase in the transport superconducting critical current density of spark-plasma sintered Bi-2223 superconductors

E. Govea-Alcaide,[1] I. F. Machado,[2] and R. F. Jardim[3,a)]
[1]*Departamento de Ciencias Básicas, Facultad de Ciencias Técnicas, Universidad de Granma, Apdo. 21, P.O. Box 85100, Bayamo, Cuba*
[2]*Departamento de Engenharia Mecatrônica e Sistemas Mecânicos, Escola Politécnica, Universidade de São Paulo, 05508-900 São Paulo, São Paulo, Brazil*
[3]*Instituto de Física, Universidade de São Paulo, CP 66318,05315-970, São Paulo, São Paulo, Brazil*

(Received 25 November 2014; accepted 14 January 2015; published online 26 January 2015)

Pre-reacted powders of $(Bi\text{-}Pb)_2Sr_2Ca_2Cu_3O_{10+\delta}$ (Bi-2223) were consolidated by using the spark plasma sintering (SPS) technique under vacuum and at two different temperatures T_D: 750 and 830 °C. The results indicate the occurrence of grains with core-shell morphology, where the shell is oxygen deficient. A post-annealing heat treatment (PAHT), performed in air, at 750 °C, and for a brief time interval, is responsible for a 10 to 25-fold increase in the transport superconducting current density at 77 K. The role of the oxygen-deficient shell, before and after the PAHT, was investigated by means of magnetic and transport measurements. We argue that the PAHT is two folds: (i) it is responsible for the decrease of the width of the oxygen-deficient shell, then increasing the oxygen content along the grain boundaries; (ii) it promotes the formation of conduction current paths along the grain boundaries of the SPS material. © *2015 AIP Publishing LLC*.
[http://dx.doi.org/10.1063/1.4906560]

I. INTRODUCTION

The spark plasma sintering (SPS) is an effective method to promote densification of powders in very short times by the simultaneous action of the electric current and the uniaxial compacting pressure.[1] Under these conditions, pre-reacted powders of superconducting $(Bi,Pb)_2Sr_2Ca_2Cu_3O_{10+\delta}$ (Bi-2223) were successfully consolidated.[2] The resulting samples were found to exhibit the same phase composition of the starting powders and reached relative densities of ∼86%, even for a low compacting pressure of 50 MPa. However, the spark plasma consolidation occurs under vacuum leading to important changes to either the normal and superconducting transport properties of the SPS materials. The combined experimental results of the specimens indicated that the surface of the grains and their grain boundaries were altered, leading to the occurrence of grains with core-shell structure comprising of: (i) a core of stoichiometric Bi-2223 phase; and (ii) an oxygen-deficient shell. Such an oxygen deficiency is responsible for the suppression of the tunneling of Cooper pairs between adjacent superconducting grains and therefore for a drastic reduction of the transport superconducting critical current J_c of the SPS materials. On the other hand, we have also found that a post-annealing heat treatment (PAHT), performed at selected temperatures and for a brief time interval of ∼5 min, was needed to partially restore the oxygen content near the surface of the grains. However, key details in the intricate balance between PATH and the general physical properties of the materials are lacking and further investigation is needed.

Within this context, the main motivation of this work is to study the role of the PAHT on the physical properties of $Bi_{1.65}Pb_{0.35}Sr_2Ca_2Cu_3O_{10+\delta}$ ceramic samples consolidated by the SPS technique. Magnetization as a function of applied magnetic field and magnetic relaxation measurements were then performed and combined with transport data in order to investigated the intra- and intergranular changes after the PAHT process.

II. EXPERIMENTAL

Polycrystalline samples of $Bi_{1.65}Pb_{0.35}Sr_2Ca_2\ Cu_3O_{10+\delta}$ (Bi-2223) were prepared by the conventional solid-state reaction method.[3] The final consolidation of the samples was performed in a SPS 1050 Dr Sinter® apparatus. In order to study the influence of the consolidation temperature, T_D, the samples were subjected to two different temperatures $T_D = 750$ and 830 °C, samples **7P** and **8P**, respectively. The heating rate was HR = 145 and 160 °C/min, respectively, and the dwell time for both samples was 5 min. Further details for producing the samples are described elsewhere.[2] The maximum uniaxial compacting pressure used in these experiments was 50 MPa. Also, the SPS samples were subjected to an additional PAHT, performed in a tubular furnace, in air, at 750 °C for 5 min. These samples, in analogy with **7P** and **8P**, are referred to **7PA** and **8PA**, respectively. For comparison reasons, ∼4 g of the starting powder was *cold pressed* inside the SPS apparatus and the resulting pellet was sintered at 845 °C in air for 2400 min. This sample (**Ref.**) will thereafter be referred as the *reference sample*.

Two types of transport measurements were performed in a closed cycle cryogenic refrigerator ARS-4HW/DE-202N attached to a temperature controller Lakeshore model 331S, and by using the standard dc four-probe technique:[3] (i) the temperature dependence of the electrical resistivity, $\rho(T)$; and (ii) the current-voltage (I–V) characteristic curves. In

a)Electronic mail: rjardim@if.usp.br

these measurements, copper electrical leads were attached to Au film contact pads of ~1400 Å in thickness, evaporated on parallelepiped-shaped samples using Ag epoxy. The typical dimensions of the samples were $t = 0.5$ mm (thickness), $w = 2$ mm (width), and $l = 10$ mm (length).

The temperature dependence of the electrical resistivity, $\rho(T)$ was measured in the temperature range 70 K $\leq T \leq$ 300 K. Before each measurement, the samples were cooled from room temperature down to 70 K. Then, an excitation current, $I = 1$ mA, was injected along the major length of the samples. Both the voltage across the sample and the temperature were collected, while the temperature was raised slowly to 300 K.

Current-voltage (I–V) measurements were performed after cooling the sample in zero applied magnetic field to $T = 77$ K. Once the temperature was stabilized, the excitation current through the sample was applied and increased automatically in steps of 1 mA, while the voltage across the sample was measured. The value of the transport critical current density at zero applied magnetic field, J_c, was determined from the measured I–V curve by taking the J_c value in which the voltage across the sample reaches 1 μV.

All magnetization measurements were performed in pellets and powder samples by using a commercial Quantum Design SQUID magnetometer. The M vs. H measurements were performed after cooling the samples down to a desired temperature in $H = 0$ Oe (zero-field-cooled ZFC condition). Once the temperature was reached, H was applied perpendicular to the compacting direction of the pellets, and increased from 0 to 1.5 T. Experimental dc magnetic susceptibility curves, $\chi = M/H$, were measured for different temperatures in the range 2–95 K in steps of ~15 K. Magnetic relaxation curves $M(t)$ were also measured in pellets and for selected temperatures between 2 and 15 K. The time dependence of M was recorded over typically 2 h.[4]

III. RESULTS AND DISCUSSION

Table I displays a summary of the transport properties of the SPS samples before and after the PAHT. The former samples exhibited very low values of the transport superconducting critical current density at $T = 77$ K in zero applied magnetic field, J_c.[2] Notice that J_c reached 2.1 A/cm^2 in the sample **8P** ($T_D = 830$ °C) and 10 A/cm^2 in **7P** ($T_D = 750$ °C). Both values are rather low when compared with the *reference sample* of 21 A/cm^2, whose relative density is ~50%. These results are close related to the parameters used in the SPS process: (i) the high consolidation temperature ($T_D > 800$ °C); (ii) the short consolidation times (~ 5 min); (iii) the low compacting pressure (50 MPa); and (iv) the vacuum (from 10 to ~30 Pa) used during the sintering.[2] The influence of (i) and (ii) on the intragranular properties of the materials seems to be small considering the other two.[2] This is not the case for the compacting pressure (50 MPa), a parameter close related to the degree of texture of the materials and very important for the intergranular medium. We have found that the degree of texture of the SPS samples is rather low, regardless of the high density of the materials. An estimate of the Lotgering factor of the SPS samples along the (00l) direction (see Ref. 5) yielded $L_{(00l)} \approx 0.1$ in all SPS samples (see, for instance, X-ray diffraction patterns of the sample 8P in Fig. 3 of Ref. 2). Thus, combining the absence of a high degree of texture and the shell-core morphology of the grains, it is reasonable to assert that SPS samples are comprised of randomly oriented grains, closely spaced, and interspersed with occasional large regions, resulting in a highly heterogeneous distribution of grain boundaries.[6,7] These features of the SPS samples are much less pronounced in the *reference sample* that has been uniaxially pressed at 50 MPa and has density close to half of the SPS samples.[2]

It is very important to mention here that J_c of our SPS samples has increased significantly after the PAHT. As displayed in Table I, J_c in sample **7P** has increased from ~10 A/cm^2 to ~128 A/cm^2 (sample **7PA**). The post-annealing heat treatment, performed at 750 °C, in air, and for 5 min, resulted in an even higher increase of J_c in sample **8P**, from ~2.1 A/cm^2 to ~58.1 A/cm^2 (sample **8PA**).[2] These results indicate a ~10 to 25-fold increase of J_c in our SPS samples and are discussed below.

The effect of the application of an external magnetic field, H, on the magnetic properties of samples comprised of a highly heterogeneous distribution of grain boundaries is then displayed in Fig. 1. In both figures, only curves measured at $T = 2$ K are displayed. The $\chi(H)$ curve of powders from the *reference sample* (Fig. 1(a)) indicates a magnetic field independent behavior up to $H_{c1g} \sim 100$ mT, and a maximum value of $|\chi_g| \sim 7$ emu/g. Such a result is close related to the magnetic flux shielding of isolated superconducting grains of the powder sample, as already observed in other superconducting cuprates.[8] Increasing magnetic field, $H > H_{c1g}$, results in the penetration of the magnetic flux within grains and the magnetic susceptibility $|\chi_g|$ decreases further and gradually. H_{c1g}, displayed in Fig. 1(a), denotes

TABLE I. Parameters extracted from the transport and magnetic measurements performed in SPS samples: the critical current density at zero applied magnetic field and $T = 77$ K, J_c, the extrapolated electrical resistivity to $T = 0$ K, $\rho(0)$, the relaxation rate, S(0), the first critical field of the intergranular medium at $T = 2$ K, $H_{c1j}(2\,\mathrm{K})$, the height of the energy barrier, U_0, the characteristic pinning length, L_c, the spatial heterogeneity factor along the grain boundary, $\tau = L_c/L_g$, the specific resistivity of the boundary, $\rho_{sp} = \rho(0)L_g$, and the product $J_c\rho_{sp}$. L_g is the mean size of the grains (see text for details).

Sample	J_c (A/cm^2)	$\rho(0)$ (mΩcm)	S(0)(10^{-3})	$H_{c1j}(2K)$ (mT)	U_0 (eV)	L_c (μm)	τ	ρ_{sp} ($\mu\Omega$cm^2)	$J_c\rho_{sp}$ (mV)
Ref.	21.8	4.6	0.51	4	0.68	1.7	0.34	2.3	0.05
7P	10.0	7.1	3.3	2.5	0.074	5.2	1.04	3.5	0.04
7PA	128.2	1.6	1.21	4	0.41	3.2	0.64	0.8	0.1
8P	2.1	24.2	3.5	< 1	0.074	15.7	3.14	12.1	0.03
8PA	58.1	1.9	1.26	3	0.36	3.6	0.72	0.95	0.06

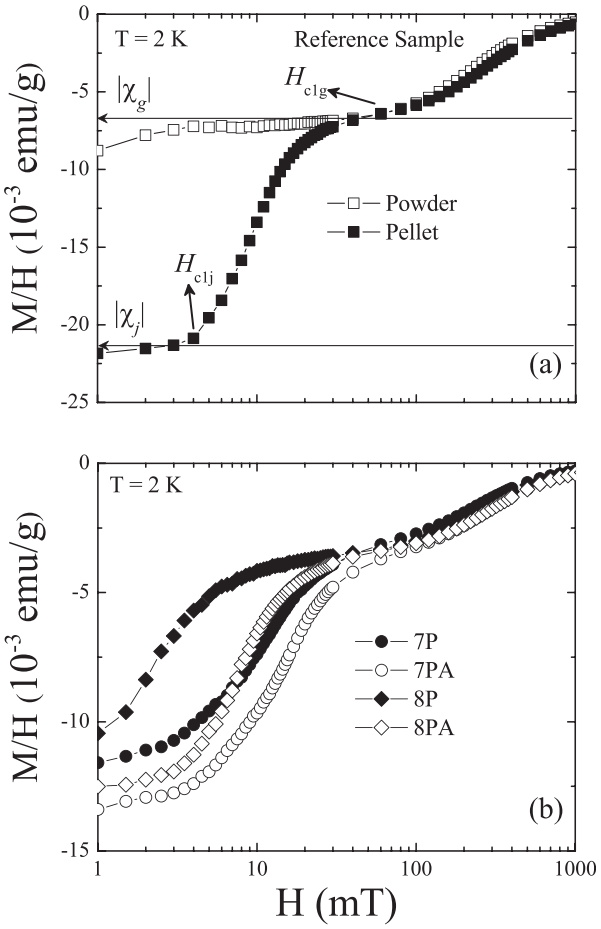

FIG. 1. Magnetic field dependence of the dc magnetic susceptibility measured at $T = 2$ K in: (a) powder and pellet of the *reference sample*; and (b) pellets of samples **7P**, **7PA**, **8P**, and **8PA**. See text for further details.

the first magnetic critical field of the superconducting grains. The $\chi(H)$ dependence of the pellet sample (*reference sample*) exhibits a quite different behaviors, indicating new intergranular features for $H < H_{c1g}$ (see Fig. 1(a)). First, χ is essentially magnetic field independent up to $H_{c1j} \sim 4$ mT, exhibiting a maximum value of $|\chi_j| \sim 22$ emu/g at H close to zero. In the magnetic-field range $4 \leq H \leq 30$ mT, $|\chi_g|$ decreases appreciably because the magnetic flux penetrates the intergranular medium of the material. For higher magnetic fields, the behavior of the $\chi(H)$ curve is very similar to that observed in the powder sample. However, it is important to point out that the low-field plateau of $\chi(H)$ observed in pellets represents the intergranular magnetic flux shielding and H_{c1j} is identified as the first intergranular critical field of the material. We also mention that due to the influence of the intergranular shielding capability, the maximum magnetic susceptibility of the pellet is close to three times greater than that measured in the powder sample, i.e., $|\chi_j| \gg |\chi_g|$.

Fig. 1(b) displays the $\chi(H)$ dependence of the SPS samples before (**7P** and **8P**) and after (**7PA** and **8PA**) the PAHT. We first notice here a smooth upward curvature of the $\chi(H)$ data in the low-magnetic field region. Such a feature is observed in three samples, except for **8P** in which a clear upward curvature of $\chi(H)$ is seen. For the three samples **7P**, **7PA**, and **8PA**, values of the first intergranular field H_{c1j} were found in the range of 2.5–4 mT, as listed in Table I. For higher fields, in the magnetic field interval $H_{c1j} \leq H \leq 40$ mT, $|\chi(H)|$ decreases in an essentially linear fashion with H. Increasing H, in the range 40 mT $\leq H \leq H_{c1g}$, the $\chi(H)$, of all samples, has a weaker magnetic field dependence, and decreases further at higher fields $H > H_{c1g}$. The combined data indicate that the PAHT has a definite influence in the intergranular media of the SPS samples. In fact, it strongly suggests that the PAHT is responsible for changes in the microstructural features of the SPS samples but important details of these changes, responsible for the above mentioned 10 to 25-fold increase of J_c still remain unclear.

To further investigate the increase of J_c after the PAHT of the SPS materials, we have performed magnetic relaxation measurements in our samples. From the time dependence of $M(t)$, the relaxation rate $S = (1/M_0)\mathrm{d}M/\mathrm{dln}t$, M_0 is the first measured value of the magnetic moment, was obtained for different temperatures and magnetic fields.[4] Figure 2 displays the S(T) dependence for all samples studied and the results reveal that S increases linearly with temperature between 2 and 15 K, indicating the occurrence of a thermally activated flux-creep process at the intergranular level. The curves were then fitted to the linear dependence $S(T) = S(0) + (k_B/U_0)T$.[4] Here, U_0 is the height of the energy barrier for the intergranular flux-creep, S(0) is the relaxation rate extrapolated to $T = 0$, and k_B is the Boltzmann constant. The results, listed in Table I, indicate that the consolidation temperature T_D has little effect on the effective pinning energy of the SPS samples. In addition to this, values of U_0 are rather low when compared with those estimated for the post-annealed samples: between samples **7P** and **7PA**, U_0 increases over five times, a value similar between samples **8P** and **8PA**. Such an increase of U_0 in the PAHT samples lends credence to the statement made above and confirms that the PAHT improves the intergranular properties of the SPS samples.

A careful inspection of Fig. 2 also indicates that all samples exhibit non-zero values for S(T) at $T = 0$. At this temperature, the general relationship for the tunnelling rate of the intergranular vortices is given by[4]

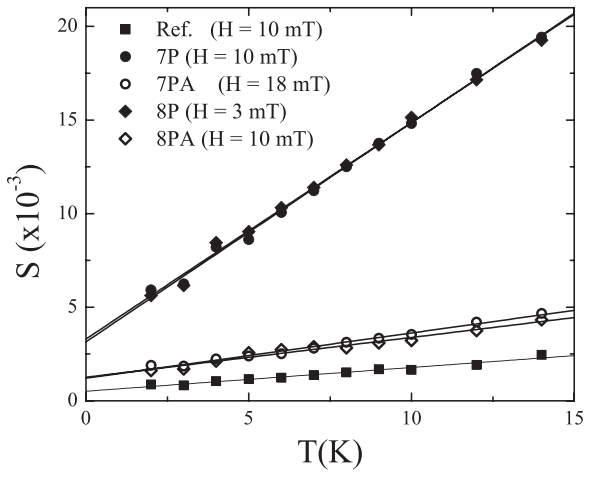

FIG. 2. Temperature dependence of the magnetic relaxation rate of the reference samples **7P**, **7PA**, **8P**, and **8PA**.

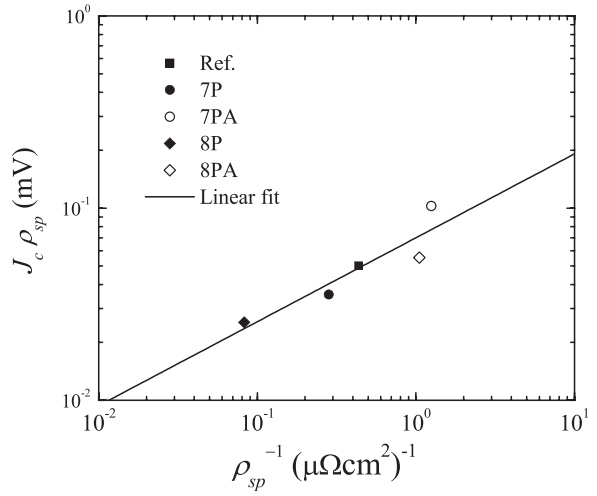

FIG. 3. Plot of $J_c\rho_{sp}$ vs. ρ_{sp}^{-1} for all samples studied in this work (see the text for details).

$$S(0) \approx \rho(0)/(R_c L_c), \tag{1}$$

where $R_c = \hbar/e^2$ is the quantum unit of the electrical resistance, L_c is the length of the intergranular pinned object along the direction of the applied magnetic field, and $\rho(0)$ is the residual electrical resistivity of the material (see Table I).[2] By using Eq. (1), values of L_c were calculated and are displayed in Table I.

The next stage of our analysis is to define the ratio $\tau = L_c/L_g$, where $L_g \sim 5\,\mu$m is the average grain size for the Bi-2223 samples.[3] Within the scenario of randomly oriented grains, closely spaced, and with core-shell morphology, τ is then used as a measure of the spatial heterogeneity of the samples along their grain boundaries, i.e., the lower the τ value, the lower is the degree of heterogeneity at the grain boundaries. In this case, heterogeneity is assumed in terms of the concentration of pinning centers along the grain boundaries. Notice that the higher is the concentration of pinning centers, the lower L_c is. As mentioned above, the SPS process results in an oxygen-deficient shell of the grains, further indicating that the oxygen concentration along grain boundaries is also highly inhomogeneous. This is particularly mirrored in the calculated values of τ of the SPS samples **7P** and **8P**, which are in the range 1 to 3 ($\tau \sim 1.04$ and 3.14, respectively), supporting the picture that grain boundaries are inhomogeneous and certainly oxygen-deficient. Within this context, the magnetic relaxation data indicate that the PAHT is efficient for restoring the oxygen concentration of the samples and for the increase of the degree of homogeneity of their grain boundaries. These features are reflected in the very low estimated values of $\tau \sim 0.64$ and 0.72 in the PAHT samples **7PA** and **8PA**, respectively.

The above analysis has its counterpart in the transport measurements. Previous studies have suggested that the electric transport across the low-oxygenated grain boundaries occurs only at selected and conductive filamentary paths, strongly sensitive to oxygen content.[6,9] Our experimental results of J_c at 77 K indicate that the number of conductive filaments at the grain boundaries of the SPS samples is rather low. Thus, besides the decrease of the width of the oxygen-deficient shell, the PAHT is also responsible for the establishment of a large number of conductive current paths, and, consequently, the reduction of the spatial heterogeneity τ along the grain boundaries of the specimens. The determination of τ is particularly important for SPS samples but much less for the *reference sample*, with very low density and a large amount of defects as porosity and voids.

A possible way to connect τ with features of the transport critical current density is by inspecting the behavior of the $J_c\rho_{sp}$ product as function of the inverse specific resistivity of the grain boundaries, ρ_{sp}^{-1}, where $\rho_{sp} = \rho(0)L_g$.[10] We have assumed here that neither SPS nor PATH processes have appreciable influence on the grain size of the samples because the intragranular properties of all samples for $H \geq H_{c1g}$ are very similar (see Fig. 1(b)). Figure 3 displays the $J_c\rho_{sp}$ data against ρ_{sp}^{-1} for all samples studied. Also, values of both $J_c\rho_{sp}$ and ρ_{sp} are listed in Table I.

The results indicate that values of the product $J_c\rho_{sp}$ are quite low ($\ll 1$ mV), while $\rho_{sp} \gg 10^{-8}\,\Omega$cm^2 assumes very high values, as expected in samples comprised of randomly oriented grains with core-shell morphology.[10–12] However, we first notice that the PAHT acts to increase the $J_c\rho_{sp}$ product over ~50%, mostly due to the reduction of the width of the oxygen deficiency shell of superconducting grains that, in turn, is responsible for the increase of the effective junction area. A careful inspection of Table I indicates that ρ_{sp} of samples **7P** and **7PA** decreases by a factor of four, from 3.5 to 0.8 $\mu\Omega$cm^2. Such a decrease in ρ_{sp} of samples **8P** and **8PA**, subjected to a higher consolidation temperature $T_D = 830\,^\circ$C and therefore much more oxygen deficient, reaches ~12 times, further indicating the effectiveness of the PAHT in restoring the oxygen content of the SPS samples. In addition to this, we have found that the experimental data follow a relation $J_c\rho_{sp} \propto \rho_{sp}^{-q}$, with $q = 0.44 \pm 0.11$. Even considering that q is universally reported to be close to 0.86,[11] the scaling found for $J_c\rho_{sp}$ may be combined with Eq. (1), resulting in the relation $J_c \propto L_c^{-1.44} \propto \tau^{-1.44}$. Actually, the above result strongly indicates that the PAHT is an effective way for decreasing the width of the oxygen-deficient shell and for altering the grain boundaries properties of the SPS materials. These combined features result in the establishment of a large number of conductive filamentary paths along the grain boundaries, further reducing their spatial heterogeneity (ascribed to both τ and ρ_{sp}), and, consequently, increasing the transport critical current density J_c of the samples. Such an increase of J_c, reaching values as high as 25 times, is then due to the establishment of conductive filamentary pathways along the reoxygenated grain boundaries of the materials.

IV. CONCLUSIONS

In summary, the role of the post-annealing heat treatment PAHT on the magnetic and transport properties of Bi-2223 samples consolidated by using the SPS method has been investigated. Reoxygenation of the SPS samples is responsible for an improvement of the spatial homogeneity of the grain boundaries, a process that is accompanied by an increase in number and the establishment of conductive filamentary paths along the grain boundaries. These changes result in 10 to 25

times increase of the superconducting critical current at 77 K. The results discussed here strongly indicated that a PATH is an important step towards increasing the transport critical current across grain boundaries in SPS ceramic samples.

ACKNOWLEDGMENTS

The authors acknowledge financial support from the Brazil's agencies FAPESP (Grant No. 2013/07296-2), CNPq (Grant No. 2014/444712-3), and CAPES/MES (Grants No. 1470/2010 and 157/2012), and the Petrobras company.

[1]R. Orrù, R. Licheri, A. M. Locci, A. Cincotti, and G. Cao, Mater. Sci. Eng., B **63**, 127 (2009).
[2]E. Govea-Alcaide, I. F. Machado, M. Bertolete-Carneiro, P. Muné, and R. F. Jardim, J. Appl. Phys. **112**, 113906 (2012).
[3]E. Govea-Alcaide, R. F. Jardim, and P. Muné, Physica C **423**, 152 (2005).
[4]S. Moehlecke and Y. Kopelevich, J. Low Temp. Phys. **106**, 207 (1997).
[5]E. Govea-Alcaide, I. García-Fornaris, P. Muné, and R. F. Jardim, Eur. Phys. J. B **58**, 373 (2007).
[6]B. H. Moeckly, D. K. Lathrop, and R. A. Buhrman, Phys. Rev. B **47**, 400 (1993).
[7]R. F. Jardim, L. Ben-Dor, D. Stroud, and M. B. Maple, Phys. Rev. B **50**, 10080 (1994).
[8]F. Pérez, X. Obradors, J. Fontcuberta, X. Bozec, and A. Fert, Supercond. Sci. Technol. **9**, 161 (1996).
[9]F. Tafuri and J. R. Kirtley, Rep. Prog. Phys. **68**, 2573 (2005).
[10]S. R. Currás, J. A. Veira, J. Maza, and F. Vidal, Supercond. Sci. Technol. **13**, 1005 (2000).
[11]S. E. Russek, D. K. Lathrop, B. H. Moeckly, R. A. Buhrman, D. H. Shin, and J. Silcox, Appl. Phys. Lett. **57**, 1155 (1990); H. Hilgenkamp and J. Mannhart, Rev. Mod. Phys. **74**, 485 (2002); J. Halbritter, Supercond. Sci. Technol. **16**, R47 (2003); R. Gross, Physica C **432**, 105 (2005).
[12]J. P. Sydow, M. Berninger, R. A. Buhrman, and B. H. Moeckly, IEEE Trans. Appl. Supercond. **9**, 2993 (1999).